Article:

Smyl, D. orcid.org/0000-0002-6730-5277, Ghasemzadeh, F. and Pour-Ghaz, M. (2016) Modeling water absorption in concrete and mortar with distributed damage. Construction and Building Materials, 125. pp. 438-449. ISSN 0950-0618

https://doi.org/10.1016/j.conbuildmat.2016.08.044

Modeling Water Absorption in Concrete and Mortar with Distributed Damage

Danny Smyl[1], Farnam Ghasemzadeh[2], and Mohammad Pour-Ghaz[1,*]

Abstract

The deterioration rate of concrete structures is directly influenced by the rate of moisture ingress. Modeling moisture ingress in concrete is therefore essential for quantitative estimation of the service life of concrete structures. While models for saturated moisture transport are commonly used, concrete, during its service life, is rarely saturated and some degree of damage is often present. In this work, we investigate whether classical isothermal unsaturated moisture transport can be used to simulate moisture ingress in damaged mortar and concrete and we compare the results of numerical simulations with experimental measurements of water sorption. The effect of hysteresis of moisture retention is also considered in the numerical simulations. The results indicate that the unsaturated moisture transport models well simulate early stages of moisture ingress at all damage levels, where capillary suction is the prominent mechanism. At later stages of moisture transport, where air diffusion and dissolution have a more significant contribution, simulations that consider moisture hysteresis compare most favorably with experimental results.

Author Keywords: Cracking; Distributed Damage; Durability; Finite Element Method; Mass Transport; Numerical Modeling; Unsaturated Mass Transport

[1] Dept. of Civil, Construction and Environmental Engineering, North Carolina State Univ., Raleigh, NC, USA.
[2] Structural Engineer, Uzan and Case, Atlanta, GA.
[*] Corresponding Author. E-mail: mpourghaz@ncsu.edu.

Field Code Changed

1. Introduction

The rate of freeze-thaw deterioration, chemical attack, corrosion of reinforcement, and many other deleterious processes in concrete structures are strongly dependent on the rate of moisture ingress. The rate of moisture ingress is heavily influenced by the degree of saturation and the presence of damage. Concrete, during its service life, is rarely saturated and some degree of damage is often present (e.g., due to freeze-thaw). Distributed damage in concrete significantly increases the rate and the amount of moisture ingress (Ghasemzadeh et al. (2016), Yang et al. (2004), Hearn (1999), Aldea et al. (1999)). While unsaturated moisture transport in concrete material has been studied (e.g. Lockington et al. (1999), Martys et al. (1997), Hall (1989)), limited research exists on unsaturated moisture transport in damaged concrete (M'Jahad et al. (2014), Wang and Ueda (2014), Mu et al. (2013), Zhou et al. (2012(a)), Zhou et al. (2012(b)), Gérard and Marchand (2000)). Specifically, modeling studies on unsaturated moisture transport in damaged cementitious material are very scarce (Van Belleghem et al. (2016), Grassl (2009), Carmeliet et al. (2004), Daïan and Saliba (1993)). In this paper, we investigate the accuracy of the classical model (including hysteresis) for simulating unsaturated water absorption in damaged mortar and concrete.

The majority of the previous studies on moisture transport in damaged cementitious material were experimental in nature. These studies have shown that, for example, chloride migration (as tested by Rapid Chloride Permeability Testing) increases in concrete after subjecting concrete to compressive loading above 75% of its compressive strength (Samaha and Hover, (1992)); Wang et al. (1997) found that water permeability generally increases with damage; Aldea et al. (1999) found that discrete cracks have a significant effect on water permeability; Rodriguez and Hooten (2003) found that chloride penetration increases in damaged samples, irrespective of the presence of mineral admixtures; Picandet et al. (2009) found that the permeability of discrete cracks increases proportional to the cube of the crack opening displacement in specimens. They also showed that the use of fiber reinforcement increases the crack tortuosity. In a recent study, the effects of distributed damage on mass transport was shown to be dependent on the mechanisms of transport considered (Ghasemzadeh and Pour-Ghaz (2014)).

The previous experimental studies have offered significant insights as to the effect of damage on the mass transport properties of damaged cement-based material. While a significant amount of experimental data for damaged cement-based materials are available in the literature, the numerical simulation of unsaturated moisture flow in damaged cement-based material is not well studied. In contrast, ~~for undamaged material,~~ numerous studies have simulated moisture flow in undamaged materials (e.g., Huang et al. (2015)), Schneider et al. (2012), Pour-Ghaz et al. (2009), Nguyen et al. (2008), and Bazant and Najjar (1972)). Numerical simulations are of significant interest since many service-life prediction models need to account for the effects of damage – characteristics which significantly affect moisture flow in concrete structures (Scherer (2015)).

Recent examples studying moisture flow simulations in damaged cementitious material include the followings. Grassl (2009) developed a lattice model, modeling 2D fractured materials, to simulate moisture flow in concrete with distributed cracks. Pour-Ghaz et al. (2009a, b) compared simulations of unsaturated moisture flow from saw-cuts, an idealized crack, to X-ray radiography images. Van Belleghem et al. (2016) compared flow regimes from numerical simulations of unsaturated moisture flow in discrete cracks with X-ray images, showing good comparison between the numerical model and X-ray images. These numerical investigations demonstrated the feasibility of numerical simulations of unsaturated moisture flow in cement-based materials. However, neither the effects of varying degrees of damage in the form of distributed cracks nor the effect of moisture retention hysteresis have been studied.

The classical model describing unsaturated mass transport in porous media is Richards' equation (Richards (1931)), modeling capillary suction. Richards' equation has been identified as a valid model for mass transport in building materials (Wilson et al. (1999)). Analytical solutions to Richards' equation have been developed for simple geometries (Cao et al. (2014), Parlange et al. (1999), Parlange et al. (1997), Warrick et al. (1991)). Analytical solutions are generally feasible in simple geometries subjected to simple boundary conditions. Practical applications, however, often requires numerical solution to Richards' equation using, for example, the Finite Element Method. The Finite Element Method solutions of Richards' equation have been used previously to analyze unsaturated moisture transport in concrete (e.g. Van Bellegham et al. (2016) and Pour-Ghaz et al. (2009a,b)). However, these studies investigated cementitious material with discrete cracks. Therefore the feasibility of using classical isothermal unsaturated moisture transport to model moisture ingress and moisture hysteresis in mortar and concrete with distributed damage remains an open question.

2 Numerical Methods

2.1 General

In this paper, moisture absorption is modeled using the Richards' Equation (Eq. 1) (Richards (1931)) for unsaturated moisture flow. Equation 1 is the classical governing differential equation for isothermal unsaturated flow

$$\frac{\partial \theta}{\partial t} = \frac{\partial}{\partial x_i}\left[K(h)\left(\frac{\partial h}{\partial x_j} + \delta_{ij}\right)\right] \qquad \text{Eq.1}$$

where $K = K(h)$ (mm/hour) is the unsaturated hydraulic conductivity, θ (mm^3/mm^3) is the volumetric moisture content, h (mm) is the capillary suction, x_i (mm) is the spatial coordinate (i,j = 1, 2, 3 for three dimensional space) and δ_{ij} is the Kronecker Delta function which accounts for the gravitational effect. Eq. 1 is generally solved using a numerical methods such as finite element method. In this work we have used a commercially available software (HYDRUS 3D) for this purpose and the details of modeling methods are discussed in Section 2.4.

2.2 Material Model

The unsaturated hydraulic conductivity (K) in Eq. 1 is a function of capillary suction (i.e., $K = K(h)$). Experimental measurements of unsaturated hydraulic conductivity are generally difficult and time consuming. These measurements are especially challenging for cement-based materials due to the fine pore size distribution resulting in high capillary suction at low water contents (Pour-Ghaz et al. (2009a,b)). Alternatively, the unsaturated hydraulic conductivity can be expressed as a product of the saturated hydraulic conductivity, K_s, and the relative hydraulic conductivity, $0 < K_r < 1.0$ (i.e., $K = K_s K_r$). Such a model, commonly used in soil physics, has been shown to well-represent the unsaturated hydraulic conductivity in cement-based materials (Schneider et al. (2012), Poyet et al. (2011), Savage and Janssen (1997)). The value of K_s can be experimentally measured using Darcy's law. The relative hydraulic conductivity is related to water content and capillary suction by Mualem's model (Mualem (1976)) (Eq. 2)

$$K_r = \Theta^l \left[\frac{\int_0^{\Theta} \frac{1}{h(x)} dx}{\int_0^{1} \frac{1}{h(x)} dx} \right]^2 \qquad \text{Eq.2}$$

Formatted: Font color: Text 1

Formatted: Font color: Text 1

Formatted: Font color: Text 1

$$\Theta = \frac{\theta - \theta_r}{\theta_s - \theta_r} \qquad \text{Eq.3}$$

where $0 \leq \Theta \leq 1.0$ is the effective material saturation, and θ_s and θ_r are the saturated moisture content and the residual moisture content, respectively. In this work, θ_s is experimentally obtained for each degree of damage and $\theta_r = 0$ (Pour-Ghaz et al. (2009a,b)). Further discussion of determining θ_s is provided in the Materials and Methods section. I is an empirical parameter which has been described as accounting for tortuosity and connectivity of pores (Mualem (1976)). Mualem proposed $I = \frac{1}{2}$ as an optimal value for 45 undisturbed soils; however, he noted that values for I can take positive or negative values. Values for soil have been shown to range from –8.83 to 100 (Schaap and Leij (2000), Yates (1992), Schuh and Cline (1990)). Kosugi argued that I has no physical significance and should be interpreted as a fitting parameter (Kosugi (1999)). Values of I for cementitious materials and especially for damaged cementitious materials are not readily available. Schneider et al. (2012) reported values of -3.0 and 35.2 for mortar and concrete, respectively. Poyet et al. (2011) concluded that the values of I can take positive or negative values, but are generally negative.

It should be noted that the choice of $\theta_r = 0$ is mainly for convenience since it does not introduce a significant modeling error and does not require elaborate measurements. In theory, the value of θ_r should correspond to the water content of the material at equilibrium with 11% relative humidity. This condition results in the formation of a monolayer of physically adsorbed moisture on calcium silicate hydrate (Alizadeh et al. 2007, Feldman and Beaudoin (1983), Feldman and Beaudoin (1976), Feldman and Sereda (1970)) which can be only achieved under extreme drying conditions. In this work, we choose $\theta_r = 0$ following

(Pour-Ghaz et al. 2009(a), 2009(b)) to also avoid inconsistency in modeling between mortar and concrete since the actual value of θ_r for concrete is unknown for our materials.

In this study, values of I are estimated by model training using maximum likelihood approach (Lay 2011). For such an approach the data need to be split into two sets: training and validation set. In this study only limited supply of experimental data is available. In such situations, using cross-validation methods may provide more accurate solutions of I. However, cross-validation methods can be very computationally expensive due to the computational cost of moisture transport simulations. We therefore use the maximum likelihood least squares fitting approach by splitting the experimental data into training and validation set using random number generators. Training set consisted of 33% of the data and validation set consisted of 67% of the entire data. Note that the training set was not used in comparison of the simulations and experiments results in the Results and Discussion section of this paper (only validation set was used). More information on the maximum likelihood least squares fitting approach can be found in (Lay (2011)).

To integrate Eq. 2, the effective saturation should be expressed as a function of capillary suction (i.e., $\Theta = \Theta(h)$). Different models for $\Theta = \Theta(h)$ have been developed (Kosugi (1996), Brooks and Corey (1964)). The model proposed by van Genuchten (1980, 1985) is used in this study and is shown in Eq. 4

$$\Theta = \frac{1}{[1+(\alpha h)^n]^m}, m = 1 - \frac{1}{n} \qquad \text{Eq.4}$$

where α and n are fitting parameters (α, inversely proportional to the mean pore diameter (mm^{-1}) and n (non-dimensional) is the curve shape parameter). These fitting parameters are obtained by fitting Eq. 4 to experimentally obtained water retention curves using the least squares method (Lay 2011). In the case of cement-based materials, instead of water retention, $\Theta = \Theta(h)$, it is more common to measure the sorption isotherm of material (i.e., $\Theta = \Theta(RH)$, RH = relative humidity). The sorption isotherm can then be converted to retention curve using Kelvin-Laplace Equation (Eq. 5) (Pour-Ghaz et al. (2009a), Leech et al. (2006), Bentz et al. (1998)):

$$h = \frac{\ln(RH)RT}{V_m} \qquad \text{Eq.5}$$

where R (J.K^{-1} mol^{-1}) is universal gas constant, T (K) is the temperature, and V_m (m^3/mole) is the molecular weight of water.

2.3 Material Model with Moisture Retention Hysteresis

The procedure for determining moisture retention curves described above is valid for both drying and rewetting of the material. However, moisture retention curves obtained using an initially-saturated specimen do not consider the effects of hysteresis. While the assumption that the parameter n remains unchanged during hysteresis has been shown to be an acceptable approximation (Nielsen and Luckner (1992), Kool and Parker (1987)), the re-wetting hydraulic parameters α^w and θ_s^w should be separately determined for the hysteresis model.

Since obtaining adsorption isotherms generally requires significant experimental time due to diffusion and dissolution of trapped air, which may be impractical in many cases, we use an analytical expression for α^w and experimental data to determine θ_s^w. In addition, we approximate that the saturated hydraulic conductivity, K_s, and tortuosity-pore connectivity parameter, I, remain the same in both drying and re-wetting. Such approximations regarding the parameters K_s and I may result in overestimation of initial sorptivity, as the magnitude of saturated hydraulic conductivity often decreases after drying (Saeidpour and Wadsö (2016), Baroghel- Bouny (2007), Mainguy et al. (2001)). Unfortunately, history-dependent data for K_s and I in damaged cementitious material are nonexistent.

The re-wetting parameter α^w is physically related to the mean pore diameter after the first drying cycle. In porous materials, α^w is generally larger than in the first drying case (i.e. $\alpha^w > \alpha$), which is largely due to air-entry into the pore system. $\alpha^w = 2\alpha$ is commonly accepted as a first approximation (Kool and Parker (1997)) and is used herein.

The saturated moisture content of a re-wetting material is less than that of the initial saturation (i.e. $\theta_s > \theta_s^w$) due to the presence of air in large pores. Here we determine θ_s^w using experimental absorption data (from the sorption test, discussed in Section 3.6). The sorption measurements beyond 90 days show negligible mass gain of the samples and, as such, it is assumed here that θ_s^w is equal to the saturated moisture content after 90 days of rewetting. While this rough approximation may lead to slight underestimation of the saturated moisture content of the rewetting material, it was found to be suitable for the hysteresis model presented. Ingress is defined as, $i = \frac{V_w}{A}$, where V_w(mm^3) and A(mm^2) are the volume of absorbed water and cross-sectional area of the absorbing specimen, respectively. If assumed to be in a completely saturated state, we can approximate $i = \frac{V_w}{A} = \frac{\theta_s^w V_s}{A}$, where V_s is the volume of the specimen. By rearranging, we obtain the expression for the re-wetting volumetric saturated moisture content: $\theta_s^w = \frac{iA}{V_s}$.

The use of hydraulic parameters θ_s^w and α^w have significant implications on the moisture retention curves of the re-wetting material. To illustrate this, Figure 1 shows drying and rewetting moisture retention curves for concrete and mortar with the highest degrees of damage. We note that the initial drying curves shown in Figure 1 were determined by using Eq. 5 to convert RH to h from the desorption isotherms. Then the complete curve was plotted by determining the fitting parameters in Eq. 4 using the experimental data. The rewetting curves were then determined for the same materials using $\alpha^w=2\alpha$ and $\theta_s^w = \frac{iA}{V_s}$.

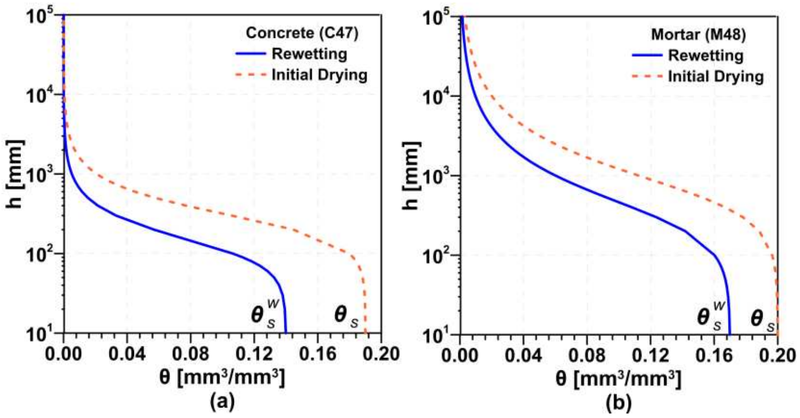

Figure 1: Drying and rewetting moisture retention curves; (a) concrete (C47) with a high degree of damage (47%) and (b) mortar (M48) with high degree of damage (48%).

2.4 Numerical Simulation and Experimental Corroboration

In this work, a commercially available Finite Element Software, HYDRUS 3D, was used (Sejna et al. (2014)). The sorption test was simulated by modeling water sorption in a 100 mm x 25 mm cylinder. Zero-flux boundary conditions were applied to all surfaces except the bottom surface were the sample was in contact with water. The boundary condition at the bottom surface was saturated boundary condition. Uniform initial moisture content, θ_i, were considered in this study; values for θ_i were experimentally obtained and are tabulated in the results section. It should be noted that the specimens used for sorption measurement were conditioned according to ASTM C1585, which does not guarantee a uniform initial moisture distribution. Achieving a uniform initial moisture distribution requires long-term conditioning, on the order of a few years (Castro (2011(a))). Therefore, in this work the simplifying assumption of uniform initial moisture condition was considered. The discussion of the effect of conditioning can be found in (Castro (2011(a))).

Finite element modeling consisted of tetrahedron elements with a maximum dimension of 1.0 mm. The finite element model was solved in terms of moisture content. The material parameters determined using the methods discussed in Section 2.2 and 2.3 (reported in Tables 2 and 3, Section 4.2) were input directly into the HYDRUS 3D.

3 Materials and Methods

3.1 Materials

Both mortar and concrete were used. Table 1 reports the mixture proportions for concrete and mortar. It should be noted that the mixture proportions reported in Table 1 are for saturated surface dry (SSD) fine and coarse aggregates. No air entraining agent was used. Entrapped air is taken in this work as a part of the open porosity. The open porosity of the hardened material can be taken as the volumetric moisture content at saturation as discussed in Hall and Hoff (2011). In this work, the volumetric moisture content at saturation was experimentally measured. For both materials, cylindrical samples with dimensions 200 mm x 100 mm (100 mm diameter) were cast. All specimens were cut into disks (25 mm x 100 mm) after 24 hours of sealed curing and then were stored for 12 months in lime saturated water. This was done to ensure uniform saturation, minimize leaching, and to uniformly mature the specimens. More detailed discussion of the benefits of lime-saturated curing may be found in (Siddiqui et al. (2013)).

Table 1: Mix proportions of concrete and mortar

Proportions	Concrete	Mortar
Cement[a] (kg/m^3)	261	609
Fly Ash, Type F (kg/m^3)	83[b]	---
Water (kg/m^3)	132.5	256
Coarse Aggregate[c] (kg/m^3)	1073	0
Fine Aggregate[d] (kg/m^3)	747	1466
Water Reducer (kg/m^3)	0.50	0.50
w/cm	0.50	0.42

[a]Ordinary Type I portland cement
[b]24% replacement by mass of cement
[c]Crushed limestone (MSA = 19 mm)
[d]Natural river sand, (FM = 2.67)
[e]Mixture proportions are for saturated surface dry (SSD) fine and coarse aggregates

3.2 Freeze-Thaw Loading

Specimens were subjected to freeze-thaw loading in an air-cooled chamber to induce different degrees of damage following the procedure in Li et al. (2011). To keep the specimens saturated during testing, they were wrapped in water-saturated cloth and sealed in a thin plastic sheet. To obtain a similar degree of damage in mortar and concrete, different temperature profiles and number of cycles were used in each material.

In concrete, the freeze-thaw cycle lasted 12 hours. Each cycle consisted of a 2-hour cooling period from 20 to -23°C, a 4-hour rest period at -23°C, a 2-hour heating period from -23 to 20°C, and a 4 hour rest period at 20°C. A maximum of 5 cycles were used in concrete.

In freeze-thaw loading of mortar, each cycle was 4 hours, including a cooling period from 21 to -35°C and a heating period to 21°C. A maximum of 25 cycles was used in mortar. Concrete specimens with five different degrees of damage (10, 21, 29, 36, and 47%) and mortar specimens with three different degrees of damage (18, 30, and 48%) were prepared. The method of quantifying damages is provided in the next section.

3.3 Quantifying Damage due to Freeze-Thaw

The degree of damage after a given number of freeze-thaw cycles was quantified using the change in dynamic elastic modulus using active acoustic emission similar to (Rashetnia et al. (2016), Ghasemzadeh and Pour-Ghaz (2014), Li et al. (2011)). Active acoustic emission describes a method in which a series of acoustic pulse (four discrete pulses in this work) is sent by an acoustic emission sensor and is captured by another sensor (pitch-catch). Then, the order of sending and receiving the pulse is switched between the two sensors. The signal transmission time is measured for all the pulses and the average value is reported (average of eight measurements). Acoustic emission sensors with a peak frequency of 375 kHz were used. Sensors were installed on opposite sides of 25 mm thick disk specimens, the perimeter of which were slightly trimmed tangent to the edge to properly install the sensors. Disk specimens were then placed on a layer of acoustic mat on a rigid, stainless steel frame. Damage was estimated based on the wave travel time in undamaged and damaged specimens and calculating the relative elastic modulus:

$$D = 1 - \frac{E_t}{E_0} = 1 - \left(\frac{t_0}{t_t}\right)^2 \quad \text{Eq.6}$$

where E_t is the dynamic elastic modulus after freeze-thaw damage, E_0 is the initial dynamic elastic modulus (before freeze-thaw damage), t_t is the signal transmission time after freeze thaw, and t_0 is the signal transmission time before freeze-thaw damage. In Eq. 6, the change in density of the damaged material is considered negligible.

3.4 Desorption Isotherm

3.4.1 Concrete

Specimens, with different degrees of damage, were conditioned at five relative humilities (50%, 65%, 75.3%, 85.1%, and 93.6%). The concrete specimens had an average mass of 52.5 g and an average thickness of 5.64 mm. The specimens were cut from the center of cylinder using a precision tile wet-saw before freeze-thaw loading. The RH values were selected from standard salt solutions: $NaCl_2$ (75.3% RH), KCl (85.1% RH), and KNO_3 (93.6% RH) following the work by Castro (2011(b)), except for the 50% and 65% RH where environmental chambers were used to fill intermediate RH values. Specimens were conditioned using saturated salt solutions, except for the 50% and 65% RH where environmental chambers were used to fill intermediate RH values. Equilibrium at a given relative humidity was defined as a change in mass less than 1.0 mg in one month. A total of three replicate specimens were used for each degree of damage (a total of 108 samples for all degrees of damage and RH). The total time required to reach equilibrium for all the samples and complete all measurements was approximately 9 months. Note that measurements were performed simultaneously. It was found that the time to reach equilibrium (regardless of the RH increment) was shorter for materials with higher degrees of damage. This may be, in part, attributed to higher porosity and higher pore connectivity of materials with a higher degrees of damage.

3.4.2 Mortar

To measure desorption isotherm of mortar specimens with different degrees of damage, an automated sorption analyzer was utilized. Small samples (0.5-1.5 mm thick, weighing 50-100 mg) were used; these samples were cut with a precision Scanning Electron Microscope wet-saw operating at 120 rpm with 5g of added mass to ensure the samples were not damaged during cutting. We note that this careful procedure was especially important at high degrees of damage, when the material had a degraded strength. These samples, with an average dimension of approximately 1 mm well represented the bulk material in absorption simulations. A discussion of the effect of sample size is provided in the Results and Discussion Section. In the sorption analyzer, mass of the specimens were monitored while the relative humidity was sequentially dropped from 97.5% to 0% RH, with a 5% RH decrease between each successive step after reaching equilibrium. Equilibrium was defined as a mass change less than 0.001 mg within 15 minutes. This criterion was previously developed, tested, and validated in the comprehensive studies by Villani et al. (2012), Castro (2011(b)), and Pour-Ghaz et al. (2010).

3.5 Saturated Hydraulic Conductivity

The saturated hydraulic conductivity (K_s) measurements were performed using an in-house developed equipment shown in Figure 2. The details of the saturated hydraulic conductivity test can be found in (Ghasemzadeh and Pour-Ghaz (2014)). Measurements were performed on initially saturated 25 mm thick disks. It is important to note that the specimens were never dried. A total of three replicates were used for concrete and a total of four replicates were used for mortar at each degree of damage.

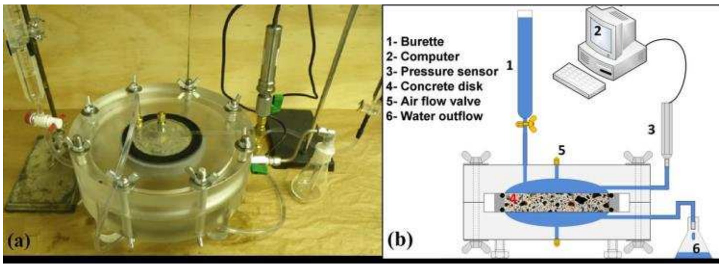

Figure 2: In-house developed equipment to measure saturated hydraulic conductivity; (a) photograph of equipment, (b) schematic of equipment implementation

3.6 Water Sorption

Sorptivity test describes the water absorption by capillary suction. To measure the amount of absorbed water by the specimen, the specimen was placed in contact with water and the mass of the specimen is monitored over time. In this work, water absorption was carried out following ASTM C1585; however, experiments were carried out up to 90 days rather than the specified 7 day testing duration. The specimen conditioning according to ASTM C1585 requires drying of the specimen at 50^{o}C. It is assumed that this drying did not induce further damage, since no large temperature gradients are present across the sample in this procedure.

Prior to the experiments, the perimeter of the specimens was sealed using epoxy. To avoid contamination of circular cross-sectional surfaces with epoxy, they were covered with pieces of paper during the application of epoxy.

3.6 Scanning Electron Microscope

Specimens analyzed by a scanning electron microscope were oven dried at 50^{o}C for 48 hours. To minimize cracking that may result from polishing and cutting, the specimens were penetrated with ultralow viscosity epoxy under a high-pressure vacuum pump (0.015 mm Hg). The epoxy-conditioned specimens were then oven cured at 50^{o}C for 10 hours followed by cutting and polishing with carbide sandpaper. The polishing consisted of sanding with low-grit to progressively higher grit sandpaper (60, 120, 240, 320, 400, 600, 800 and 1,200 grit) and half-micron diamond suspension. The backscattered mode was used for SEM imaging with pressure and accelerating voltage of 30 Pa and 20 kV, respectively.

4. Results and Discussion

4.1 Freeze-Thaw Damage Visualization and Detection

SEM images for six degrees of damage are shown in Figure 3, the left column shows SEM images of concrete and the right column shows SEM images of mortar. These images are provided to visualize damage in the materials. In the images shown, it is clear that freeze-thaw damage is distributed across the cement paste phase, although some fractures are observed along the aggregate boundaries. As damage increases, the fractures become interconnected and wider in both mortar and concrete. In Figure 3, fracture widths, in all degrees of damage, are below 25μm. However, pore sizes, for cement paste in general, range from nanometers to approximately 0.05μm (Lura et al. (2003)). The mortar specimen sizes used in this work for obtaining desorption isotherms are, at a minimum 100-2,500 times larger in dimension than the distributed pore or fracture systems. Consistent with representative volume element (RVE) size discussed by Nemat-Nasser and Hori (1995), the specimen sizes used for desorption isotherms of mortar are much larger than the microstructure, and therefore, well-represent bulk material properties. By the same argument, the use of desorption analyzer was deemed inappropriate for measuring desorption isotherms of concrete due to the large aggregate sizes. Indeed, the concrete specimens tested here had aggregates with a maximum size of 19 mm, resulting in a much larger RVE size than mortar.

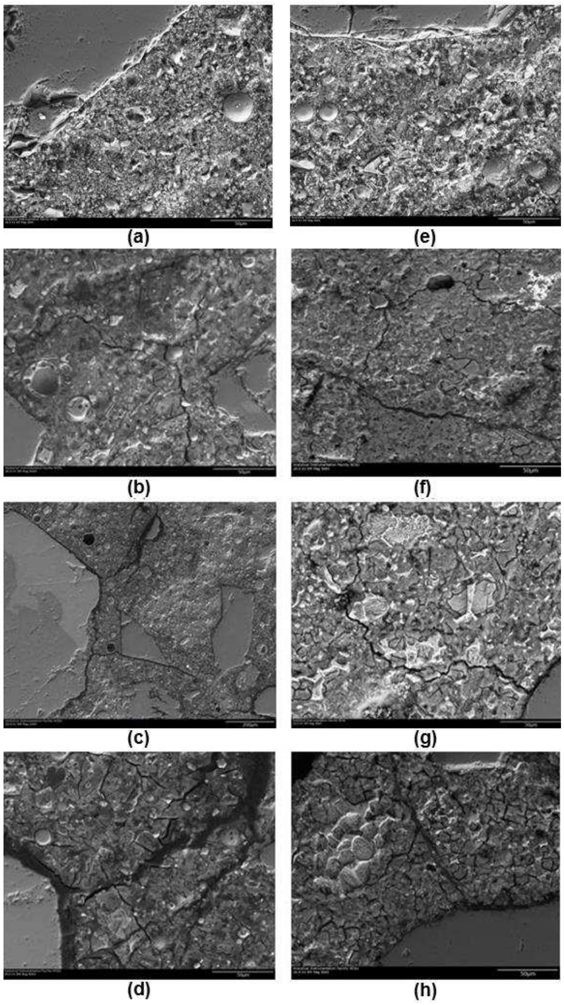

Figure 3: Representative SEM images of concrete with (a) D = 0%, (b) D = 21%, (c) D = 29%, (d) D = 47%; and mortar with (e) D = 0%, (f) D = 18%, (g) D = 30%, and (h) D = 48%

The damage shown in the material depicted in Figure 3 was quantified using the change in elastic properties using active acoustic emission methods. In Figure 4, the measured degrees of damage using active emission for both mortar and concrete are reported. The error bars in Figure 4 represent standard deviation. The degree of damage in mortar and concrete increases linearly with the number of freeze-thaw cycles.

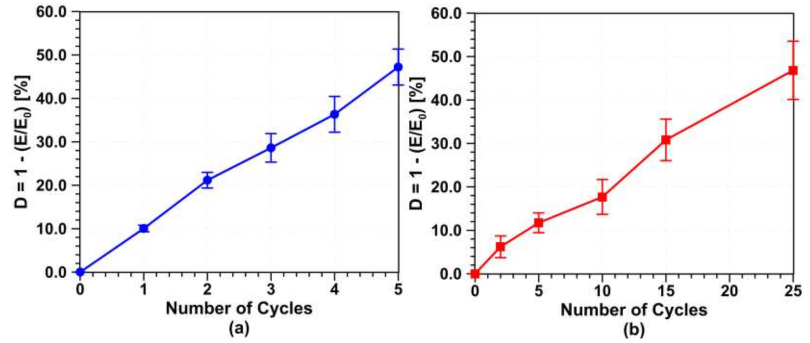

Figure 4: Degree of Damage, D (%), based on the reduction of elastic modulus using acoustic emission; (a) concrete, (b) mortar

4.2 Material Parameters

Figures 5a and 5b show the measured desorption isotherms for mortar and concrete specimens, respectively. The desorption isotherms of mortar have a higher number of data points and a wider range of RH values, as compared to that of concrete, since they were measured using an automated sorption analyzer.

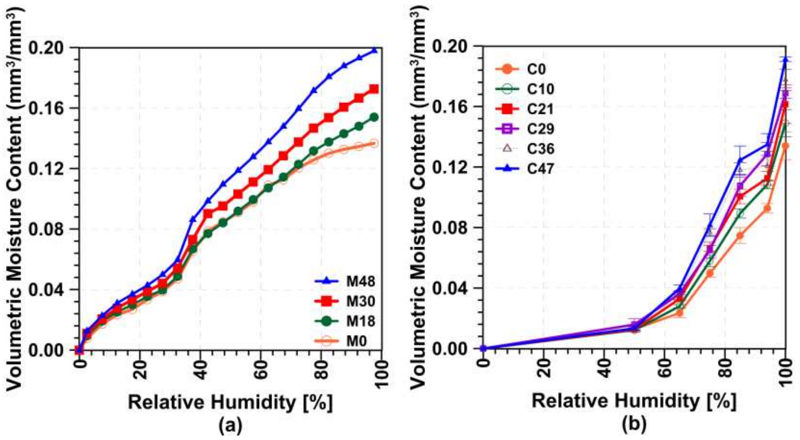

Figure 5: Desorption isotherm of specimens with different degrees of damage; (a) mortar, (b) concrete. “M” and “C” denote mortar and concrete, respectively, and the number following these letters indicate the ~~is the~~ degree of damage (%).

For both materials the isotherms shift upward with increased damage, indicating damage increases porosity over a wide range (Ghasemzadeh and Pour-Ghaz (2014)). The van Genuchten model (Eq. 4) was fit to these isotherms, after converting them to water retention curves using Eq. 5. The van Genuchten model parameters for mortar and concrete are reported in Tables 2 and 3 respectively. The values for saturated hydraulic conductivity (K_s), saturated moisture content (θ_s), empirical parameter I, and the rewetting parameters (θ_s^w and α^w) are also reported in Tables 2 and 3. In Tables 2 and 3 “C” and “M” stand for concrete and mortar respectively, and the number following these letters indicates the degree of damage.

Table 2: Saturated hydraulic conductivity, saturation water content, and van Genuchten model parameters for mortar specimens

Identifier	Damage	K_s	α	α^w	n	I	θ_i	θ_s	θ_s^w
-	%	mm/hr	1/mm	1/mm	-	-	-	-	-
M0	0	3.0×10^{-5}	1.2×10^{-2}	2.4×10^{-2}	2.06	-9.0	0.03	0.14	0.10
M18	18	59.0×10^{-5}	1.8×10^{-2}	3.6×10^{-2}	1.75	-8.0	0.01	0.15	0.14
M30	30	194.0×10^{-5}	3.3×10^{-2}	6.6×10^{-2}	1.52	-8.0	0.02	0.17	0.15
M48	48	341.0×10^{-5}	1.7×10^{-2}	3.4×10^{-2}	1.81	-8.0	0.01	0.20	0.17

Table 3: Saturated hydraulic conductivity, saturation water content, and van Genuchten model parameters for concrete specimens

Identifier	Damage	K_s	α	α^w	n	I	θ_i	θ_s	θ_s^w
-	%	mm/hr	1/mm	1/mm	-	-		-	-
C0	0	1.4×10^{-4}	6.4×10^{-2}	1.3×10^{-1}	2.26	-7.0	0.03	0.15	0.11
C10	10	7.0×10^{-4}	4.9×10^{-2}	9.8×10^{-2}	2.45	-7.0	0.03	0.15	0.11
C21	21	14.0×10^{-4}	4.6×10^{-2}	9.2×10^{-2}	2.47	-7.0	0.04	0.16	0.11
C29	29	26.0×10^{-4}	4.6×10^{-2}	9.2×10^{-2}	2.48	-6.0	0.03	0.17	0.12
C36	36	56.0×10^{-4}	4.1×10^{-2}	8.2×10^{-2}	2.64	-5.0	0.03	0.18	0.13
C47	47	131.0×10^{-4}	4.3×10^{-2}	8.6×10^{-2}	2.58	-5.0	0.03	0.19	0.14

We would like to point out here that while Mualem (Mualem (1976)) proposed the parameter I to account for tortuosity and pore connectivity, such a physical interpretation may be only meaningful if $I \geq 0$ in the classical model of unsaturated hydraulic conductivity (Durner 1994). In this study, using the approach described in Section 2.2, satisfactory results were found for negative values similar to the works in (Schneider et al. (2012), Poyet et al. (2011), Schaap and Leij (2000), Yates (1992), and Schuh and Cline (1990)).

In addition to I, the saturated hydraulic conductivity (K_s) and open porosity (θ_s) have significant effects on the sorptive behavior of cement-based materials. In particular, K_s considerably influences initial sorptivity. K_s is shown in Figure 6a to increase with the degree of damage in both mortar and concrete. Figure 6b shows that θ_s increases with damage, similar to the increase of porosity observed in desorption isotherms. θ_s (or θ_s^w in the case of hysteresis) largely influences the final magnitude of moisture ingress and the duration of initial absorption. While the values of open porosity in mortar and concrete are similar in magnitude, K_s of concrete is significantly higher than that of mortar, especially at higher degrees of damage. This indicates that the open porosity (pores and fractures) are better connected in concrete as compared to mortar.

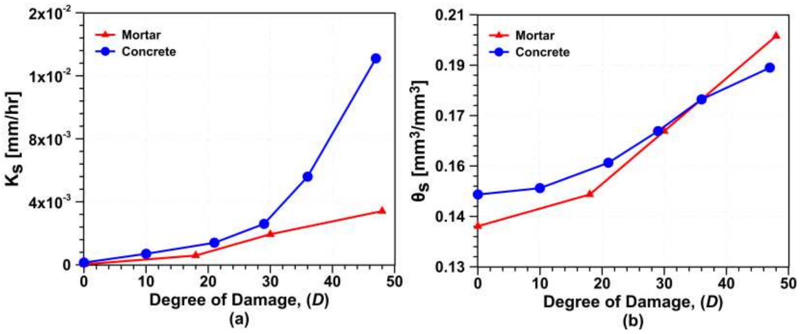

Figure 6: Effect of damage, D (%), on (a) saturated hydraulic conductivity and, (b) open porosity, θ_s, in mortar and concrete.

4.3 Simulation of Unsaturated Moisture Transport in Mortar

Results of the experimental measurements and numerical simulations of water absorption of mortar with different degrees of damage are compared in Figure 7. Simulations of water absorption using the material model without hysteresis (from the desorption isotherm) and the proposed material model including hysteresis are included. The results are presented as volume of water (mm^3) absorbed per water absorbing surface (mm^2) of the sample versus square root of time ($day^{1/2}$). The results were compared for the first 90 days. Note that for each degree of damage, simulation results are compared with experimental results from two samples.

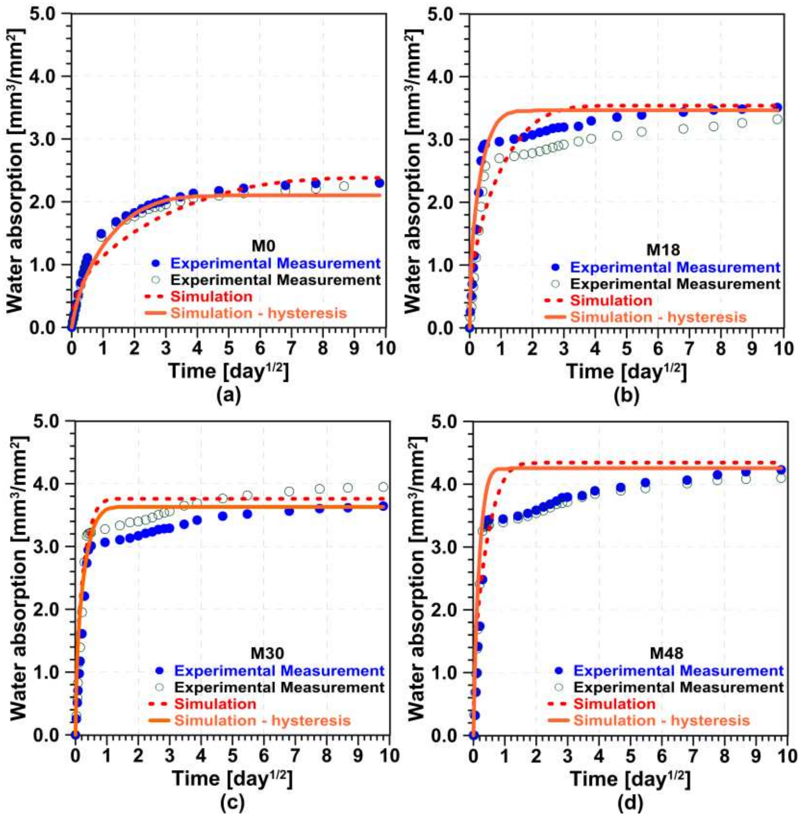

Figure 7: Experimental and numerical sorption results for mortar specimens with different degrees of damage; a) D = 0%, b) D = 18%, c) D = 30%, d) D = 48%

In Figure 7, for all degrees of damage, the results of simulations of water absorption in mortar compare well with experimental results at early stages of water absorption. In simulations where hysteresis is considered, early-stage results more closely match experimental results. The slope of the first linear portion of the experimental and numerical results, initial sorptivity, is calculated and plotted as a function of degree of damage in Figure 8. Figure 8 confirms that the results of simulation for the initial stages of water absorption agree well with experimental results, particularly in simulations where hysteresis is considered.

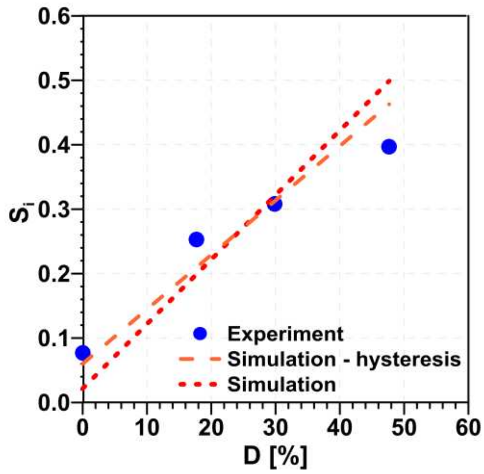

Figure 8: Comparison of experimentally and numerically obtained initial sorptivity, S_i, of mortar as a function of damage

In Figure 7, at later stages of water absorption, simulation results deviate from the experimental results. The deviation increases with damage level. As the damage increases, a sharp "knee point" appears in both experimental and numerical results. There is, however, a distinct difference between the numerical and experimental results after the knee point. In simulated results the sharp transition marks the transition from unsaturated to saturated state of the sample while in experimental results the specimen continues to absorb water after the knee point. In experimental results, the knee point marks transition from capillary suction to air diffusion and dissolution mechanism of water absorption (Ghasemzadeh et al. (2016), Ghasemzadeh and Pour-Ghaz (2014)). Since Richards' Equation does not account for air diffusion and dissolution mechanisms, in simulation results (Figure 7), the specimen continues to absorb water with capillary suction until saturation (Li et al. (2016)). However, in experimental results, the specimen continues to absorb water after the knee point, largely due to the effects of air diffusion and dissolution mechanisms.

4.4 Simulation of Unsaturated Moisture Transport in Concrete

Results of the experimental measurements and numerical simulation of water absorption in concrete with different degrees of damage are compared in Figure 9. Simulation results considering hysteresis are also reported. Similar to the results for mortar specimens, the results are compared for the first 90 days. Note that for each degree of damage, simulation results are compared with experimental results from two samples.

The results in Figure 9 are similar to the results presented in Figure 7. At early stages of water absorption, the simulation and experimental results agree well while they diverge at later stages of water absorption. Simulations considering moisture hysteresis are shown to more closely match experimental results in both late- and early-stages of moisture. This is largely due to the improved estimation (relative to using drying data) of saturated moisture content after drying.

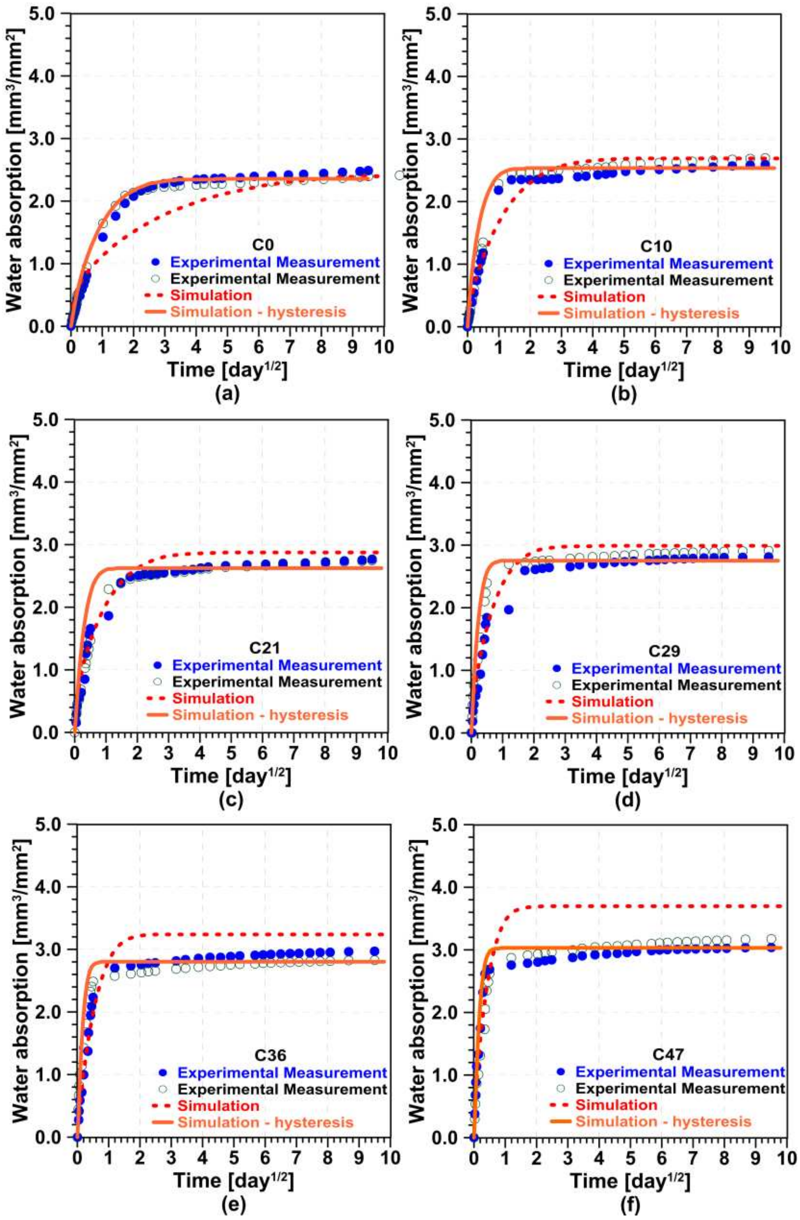

Figure 9: Experimental and numerical sorption results for concrete specimens with different degrees of damage; a) D = 0%, b) D = 10%, c) D = 21%, d) D = 29%, e) D = 36%, f) D = 47%

Figure 10, similar to Figure 8, compares the initial sorptivity calculated from experimental and numerical results. Again, Figure 10 confirms that the results of simulation for the initial stages of water absorption agree well with experimental results. Considering the effect of hysteresis in the simulations significantly improves the estimation of initial sorptivity at higher degrees of damage.

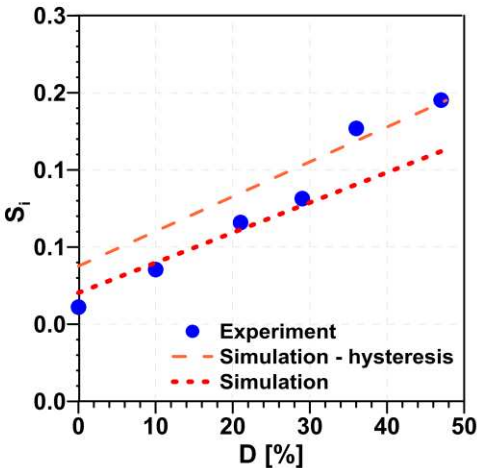

Figure 10: Comparison of experimentally and numerically obtained initial sorptivity, S_i, of concrete as a function of damage

4.5 Discussion of Unsaturated Moisture Absorption Modeling Using the Classical Isothermal Model

Simulation of moisture ingress using Richards' Equation only describes the physics of capillary suction. For cementitious material with distributed damage, the accuracy of simulation results is highly dependent on the experimentally obtained isotherms and hydraulic parameters. In particular, the value of saturated hydraulic conductivity and open porosity significantly affect the simulation results. The advantages of using the simulation techniques presented in this paper are (i) the material parameters are directly measured using well-researched and well-developed experimental techniques, (ii) simulation of moisture absorption using Richards' Equation requires relatively few modeling parameters, and (iii) the material model considering hysteresis does not require the adsorption isotherm – the acquisition of which may require considerable experimental time.

However, the simulation techniques presented herein have some limitations. The simple moisture hysteresis model does induce some uncertainty, since modeling parameters do not originate from the adsorption isotherm. Moreover, in the modeling approach used here, "homogenized" material parameters are used which account for the overall contribution of matrix and fractures, and therefore, this model neglects direct simulation of matrix-fracture moisture transfer. While early-stage simulation results were generally satisfactory, neglecting matrix-fracture interaction and air diffusion/dissolution lead to the divergence of simulation results from experimental results in late-stages of water absorption where hysteresis is not considered. To improve simulation results at late-stages of water absorption, especially at high levels of saturation and damage, the feasibility of advanced models such as dual-permeability or dual-porosity should be studied. Furthermore, models for air-diffusion and dissolution may improve simulations of late-stage moisture absorption.

5. Conclusion

In this work, a classical isothermal unsaturated moisture transport model was used to simulate moisture ingress in mortar and concrete with a wide range of damage. In the material model where hysteresis was not considered, material parameters were obtained from experimental measurements. For the material model accounting for hysteresis, material parameters were developed based off experimental and analytical means. The results indicate that, for all levels of damage, the classical isothermal unsaturated moisture transport model well simulates the early stages of moisture ingress in mortar and concrete where capillary suction is the underlying mechanism. At later stages where air diffusion and dissolution mechanisms as well as matrix-fracture interaction play a more significant role, the results of simulations excluding the effects of hysteresis deviate from experimental measurements. In contrast, results of late-stage water absorption in simulations considering hysteresis more closely match experimental results. The use of more advanced material models might be necessary to obtain more accurate results at later stages of water absorption.

Acknowledgment

This work was conducted in the Materials and Sensor Development Laboratory (MSDL), Constructed Facilities Laboratory (CFL), and the Analytical Instrumentation Facility (AIF) at North Carolina State University. The authors would like to acknowledge the support which has made these laboratories and this research possible. The authors would like to acknowledge the contributions of the technical staff of CFL, Dr. Gregory Lucier, Mr. Jonothan McEntire, and Mr. Jerry Atkinson as well as the contributions of technical staff of AIF, Mr. Chuck Mooney and Mr. Roberto Garcia. The first and second authors of this paper were, in part, supported by the Department of Civil Construction and Environmental Engineering at North Carolina State University. This support is greatly acknowledged.

References

Aldea, C., Shah, S., and Karr, A. (1999). “Effect of cracking on water and chloride permeability of concrete.” Journal of Materials in Civil Engineering., 11, 181-187.

Alizadeh, R., Beaudoin, J. J., and Raki, L. (2007). “C–S–H (I)—A Nanostructural Model for the Removal of Water from Hydrated Cement Paste?” Journal of the American Ceramic Society, 90(2), 670-672.

Baroghel-Bouny, V. (2007). “Water vapour sorption experiments on hardened cementitious materials. Part II: Essential tool for assessment of transport properties and for durability prediction.” Cement and Concrete Research., 37(3), 438-454.

Bentz, D. P., Garboczi, E. J., and Quenard, D. A. (1998). “Modelling drying shrinkage in reconstructed porous materials: application to porous Vycor glass.” Modelling and Simulation in Materials Science and Engineering, 6(3), 211.

Brooks, R. H., and A. T. Corey. (1964). “Hydraulic properties of porous media.” Hydrology Paper 3, Colorado State University, Fort Collins, Colorado.

Carmeliet, J., Delerue, J. F., Vandersteen, K., and Roels, S. (2004). “Three-dimensional liquid transport in concrete cracks.” International journal for numerical and analytical methods in geomechanics, 28(7-8), 671-687.

Cao, H. and Yue, X. (2014). “Homogenization of Richards’ equation of van Genuchten–Mualem model.” Journal of Mathematical Analysis and Applications., 412(1), 391-400.

Castro, J., Bentz, D. and Weiss, J. (2011(a)). “Effect of sample conditioning on the water absorption of concrete”, Cement and Concrete Composite, 33 (8), 805-813.

Castro, J. (2011(b)). “Moisture transport in cement based materials: application to transport tests and internal curing.” PhD Thesis., Purdue University, Indiana.

Daïan, J. F., and Saliba, J. (1993). “Transient moisture transport in a cracked porous medium.” Transport in porous media, 13(3), 239-260.

Durner, W. (1994). “Hydraulic conductivity estimation for soils with heterogeneous pore structure.” Water Resources Research. 30(2), 211-223.

Feldman, R. F., and Beaudoin, J. J. (1983). “Effect of applied stress on the helium inflow characteristics of hydrated Portland cement. Cement and Concrete Research, 13(4), 470-476.”

Feldman, R. F., and Beaudoin, J. J. (1976). Microstructure and strength of hydrated cement. Cement and Concrete Research, 6(3), 389-400.

Feldman, R. F., and Sereda, P. J. (1970). A new model for hydrated Portland cement and its practical implications. Engineering Journal, 53(8/9), 53-59

Ghasemzadeh, F., Rashetnia, R., Smyl, D., and Pour-Ghaz, M. (2016). A comparison of methods to evaluate mass transport in damaged mortar. Cement and Concrete Composites, 70, 119-129.

Ghasemzadeh, F. and Pour-Ghaz, M. (2014). “The effect of damage on moisture transport in concrete.” Journal of Material in Civil Engineering., DOI: 10.1061/(ASCE)MT.1943-5533.0001211.

Gérard, B., & Marchand, J. (2000). “Influence of cracking on the diffusion properties of cement-based materials: Part I: Influence of continuous cracks on the steady-state regime. Cement and Concrete Research.” 30(1), 37-43.

P. Grassl. (2009). “A lattice approach to model flow in cracked concrete.” Cement and Concrete Composites. 31(7), 454-460.

Hall, C. (1989). “Water sorptivity of mortars and concrete: a review.” Magazine of Concrete Research., 41(147), 51–61.

Hall, C., and Hoff, W. (2011). “Water transport in brick, stone, and concrete.” London and New York. Second Version.

Hallaji, M., Seppanen, A., and Pour-Ghaz, M. (2015). “Electrical resistance tomography to monitor unsaturated moisture flow in cementitious materials.” Cement and Concrete Research., 69, 10-18.

Hearn, N. (1999). “Effect of shrinkage and load-induced cracking on water permeability of concrete.” ACI Materials Journal., 96(2), 234–240.

Huang, Q., Jiang, Z., Gu, X., Zhang, B., and Goi, B. (2012). “Numerical simulation of moisture transport in concrete based on a pore size distribution model.” Cement and Concrete Research., 67, 31-43.

Kool, J.B. and Parker, C. (1987) “Development and evaluation of closed-form expressions for hysteretic soil hydraulic properties.” Water Resources Research. 23(1), 105-114.

Kosugi, K. (1996). “Lognormal distribution model for unsaturated soil hydraulic properties.” Water Resources Research., 32(9), 2697-2703.

Kosugi, K. (1999). “General model for unsaturated hydraulic conductivity for soils with lognormal pore-size distribution.” Soil Science Society of America Journal., 63, 270-277.

Lay, D. C., (2011) “Linear algebra and its applications.” Pearson Education, Inc. Boston, Massachusetts. Fourth Edition.

Leech, C., Lockington, D., Hooton, R. D., Galloway, G., Cowin, G., and Dux, P. (2008). “Validation of mualem’s conductivity model and prediction of saturated permeability from sorptivity.” ACI Materials Journal., 105(1), 44-51.

Li, W., Pour-Ghaz, M., Trtik, P., Wyrzykowski, M., Münch, B., Lura, P., Vontobel, P., Lehmann, E., and Weiss, J. (2016). “Using neutron radiography to assess water absorption in air entrained mortar.” Construction and Building Materials, 110, 98-105.

Li, W., Pour-Ghaz, M., Castro, J., and Weiss, J., (2012). “Water absorption and critical degree of saturation relating to freeze-thaw damaged in concrete pavement joints.” Journal of Materials in Civil Engineering., 24(3), 299-307.

Lockington, D., Parlange, J., Y., and Dux, P. (1999). “Sorptivity and the estimation of water penetration into unsaturated concrete.” Materials and Structures., 32, 342–347.

Lura, P., and Jensen, O. M., and van Breugel, K. (2003) “Autogenous shrinkage in high-performance cement paste: an evaluation of basic mechanisms.” Cement and Concrete Research., 33, 223-232.

M’Jahad, S., Davy, C. A., Bourbon, X., and Skoczylas, F. (2014). “Water Retention and Gas Migration of Two High-Performance Concretes after Damage.” Journal of Materials in Civil Engineering, 27(2), A4014008.

Formatted: Font color: Text 1

Mainguy, M., Coussy, O., and Baroghel-Bouny (2001) “Role of air pressure in drying of weakly permeable materials.” Journal of Materials in Civil Engineering., 127(6), 582-592.

Martys, N. and Ferraris, C. (1997). “Capillary transport in mortars and concrete.” Cement and Concrete Research., 27(5),747-760.

Mualem, Y. (1976). “A new model for predicting the hydraulic conductivity of unsaturated porous media.” Water Resources Research., 12(3), 513-513.

Mu, S., De Schutter, G., & Ma, B. G. (2013). “Non-steady state chloride diffusion in concrete with different crack densities.” Materials and Structures, 46(1-2), 123-133.

Nemat-Nasser, S. and Hori, M. (1995). “Micromechanics: overall properties of heterogeneous materials.” Elsevier Science Publishers.

Nguyen, T., Petocic, J., Dangia, P., and Baroghel-Bouny, V. (2008). “ Modeling of coupled ion and moisture transport in porous building materials.” Construction and Building Materials., 22, 2185-2195.

Nielsen, D.R. and Luckner, L. (1992). “Theoretical aspects to estimate reasonable initial parameters and range limits in identification procedures for soil hydraulic properties.” Proc. Intl. Workshop on Indirect Methods for Estimating the Hydraulic Properties of Unsaturated Soils. University of California, Riverside.

Parlange, J., Barry, D., Parlange, M., Hogarth, W., Haverkamp, R., Ross, P., and Steenhuis, T. (1997). “New approximate analytical technique to solve Richards Equation for arbitrary surface boundary conditions.” Water Resources Research., 33(4), 903-903.

Parlange, J., Hogarth, W., Barry, D., Parlange, M., Haverkamp, R., Ross, P., and Katul, G. (1999). “Analytical approximation to the solutions of Richards' equation with applications to infiltration, ponding, and time compression approximation.” Advances in Water Resources., 23(2), 189-194.

Formatted: Indent: First line: 0"

Formatted: Font color: Text 1

Picandet V., Khelidj A., and Bellegou, H. (2009). “Crack effects on gas and water permeability of concretes.” Cement and Concrete Research. 39(6), 537-547.

Pour-Ghaz, M. (2011). “Detecting damage in concrete using electrical methods and assessing moisture movement in cracked concrete.” PhD Thesis, Purdue University, Indiana.

Pour-Ghaz, M., Rajabipour, F., Couch, J., and Weiss, J. (2009(a)). “Numerical and experimental assessment of unsaturated fluid transport in saw-cut (notched) concrete elements.” American Concrete Institute (ACI) Special Publication 266, Farmington Hills, MI., 73–86.

Pour-Ghaz, M., Rajabipour, F., Couch, J., and Weiss, J. (2009(b)). “Modeling fluid transport in cementitious systems with crack-like (notch) geometries.” Proceedings of the 2nd International RILEM Workshop on Concrete Durability and Service Life Planning, Haifa, Israel.

Pour-Ghaz, M., Spragg R., and Weiss J. (2010). “Moisture profiles and diffusion coefficients in mortars containing shrinkage reducing admixtures.” International RILEM Conference on Use of Superabsorbent Polymers and Other New Additives in Concrete. Technical University of Denmark, Lyngby, Denmark., 197-206.

Poyet, S., Charles, S., Honore, N., and L’hostit, V. (2011). “Assessment of unsaturated water transport properties in an old concrete: determination of the pore-interaction factor.” Cement and Concrete Research., 41(10), 1015-1023.

Rashetnia, R., Ghasemzadeh, F., and Pour-Ghaz, M. (2016). “The Consequences of Material Nonlinearity on the Axisymmetric Flexural Vibration Measurements for Estimating the Dynamic Elastic Modulus of Damaged Cement Based Materials.” Journal of Advanced Concrete Technology, 14(6), 287-298

Richards, L. A. (1931). “Capillary conduction of liquids through porous mediums.” Physics., 1, 318-333.

Rodriguez O. G. and Hooton R. D. (2003). “Influence of cracks on chloride ingress into concrete.” ACI Materials Journal., 100(2), 120-126.

Samaha, H. R. and Hover, K. (1992). “Influence of microcracking on the mass transport properties of concrete.” ACI Materials Journal., 89(4), 416-424.

Savage, B. and Janssen, D. (1997). “Soil physics principles validated for use in predicting unsaturated moisture movement in Portland cement concrete.” ACI Materials Journal, 94(1), 63-70.

Schaap, M. and Leij, F. (2000). “Improved prediction of unsaturated hydraulic conductivity with the Maulem-van Genuchten model.” Soil Science Society of America Journal., 64(3), 843-851.

Scherer, G. (2015). “Drying, shrinkage, and cracking of cementitious materials.” Transport in Porous Media., 110(2), 311-331.

Schuh, W. M. and Cline, R. L. (1990). “Effect of soil properties on unsaturated hydraulic conductivity pore-interaction factors.” Soil Science Society of America Journal., 54(6), 1509-1519.

Schneider, S., Mallants, D., and Jacques, D. (2012). “Determining hydraulic properties of concrete and mortar by inverse modeling.” Materials Research Society Symposium.

Sejna, M., Simunek, J., and van Genuchten, M. Th. (2014). “The HYDRUS software package for simulating the two- and three-dimensional movement of water, heat, and multiple solutes in variably-saturated porous media.” http://www.pc-progress.com/en/..%5Cdownloads%5CPgm_Hydrus3D2%5CHYDRUS3D%20User%20Manual.pdf.

Saeidpour, M. and Wadsö, L. (2016) “Moisture diffusion coefficients of mortars in absorption and desorption.” Cement and Concrete Research. 83, 179-183.

Siddiqui, M.S., Nyberg, W., Smith, W., Blackwell, B., and Riding, K. (2013) “Effect of curing water availability and composition on cement hydration.” ACI Materials Journal., 110(3), 315-322.

Van Belleghem, B., Montoya, R., Dewanckele, J., Van den Steen, N., De Graeve, J., Deconinck, J., Cnudde, V., Van Tittelbloom, K., and De Belie, N. (2016) “Capillary water absorption in cracked and uncracked mortar – A comparison between experimental study and finite element analysis.” Construction and Building Materials., 110(1), 154-162.

Van Genuchten, M. Th. and Nielsen, D. R. (1985). “On describing and predicting the hydraulic properties of unsaturated soils.” Annals of Geophysics., 3(5), 615-628.

Van Genuchten, M. Th. (1980). “A closed-form equation for predicting the hydraulic conductivity of unsaturated soils.” Soil Science Society of America Journal., 44(5), 892-898.

Villani, C., Spragg, R., Pour-Ghaz, M., and Weiss, J. (2014). “The influence of pore solutions properties on drying in cementitious materials.” Journal of the American Ceramic Society., 97(2), 386-393.

Villani, C., Spragg, R., Pour-Ghaz, M., and Weiss, J. (2012). The role of deicing salts on the non-linear moisture diffusion coefficient of cementitious materials during drying.” In Proc., Int. Symp. on Brittle Matrix Composites (pp. 1-14). Institute of Fundamental Technological Research of the Polish Academy of Sciences, Warsaw, Poland.

Wang, K., Jansen, D. C., Shah, S. P., and Karr, A. F. (1997). “Permeability study of cracked concrete.” Cement and Concrete Research., 27, 381–393.

Wang L., and Ueda, T. (2014). “Mesoscale modelling of the chloride diffusion in unsaturated concrete damaged by freeze-thaw cycling.” Journal of Material in Civil Engineering., 26(5), 955-965.

Warrick, A., Islas, A., and Lomen, D. (1997). “An analytical solution to Richards' equation for time-varying infiltration.” Water Resources Research., 27(5), 763-766.

Wilson, M., Carter, M., and Hoff, W. (1999). "British standard and RILEM water absorption tests: A critical evaluation." Materials and Structures., 32, 571-578.

Yang, Z. (2004). "Assessing cumulative damage in concrete and quantifying its influence on life cycle performance modeling." Ph.D. thesis, Purdue University, West Lafayette, Ind.

Yang, Z., Weiss, J., and Olek, J. (2006). "Water transport in concrete damaged by tensile loading and freeze–thaw cycling." Journal of Materials in Civil Engineering., 18(3), 424-424.

Yates, S. R., Van Genuchten, M. Th., Warrick, A.W., and Leij, F. J. (1992). "Analysis of measured, predicted, and estimated hydraulic conductivity using RETC computer program." Soil Society of America Journal., 56, 347-354.

Zhou, C., Li, K., and Han, J. (2012a). "Characterizing the effect of compressive damage on transport properties of cracked concretes." Materials and Structures, 45(3), 381-392.

Zhou, C., Li, K., & Pang, X. (2012b). "Geometry of crack network and its impact on transport properties of concrete." Cement and Concrete Research, 42(9), 1261-1272.

Formatted: Font color: Text 1